MOLECULAR BIOLOGY

RHINO directs MMEJ to repair DNA breaks in mitosis

Alessandra Brambati[1]*†, Olivia Sacco[1]†, Sarina Porcella[1]†, Joshua Heyza[2,3], Mike Kareh[1], Jens C. Schmidt[2,3], Agnel Sfeir[1]*

Nonhomologous end-joining (NHEJ) and homologous recombination (HR) are the primary pathways for repairing DNA double-strand breaks (DSBs) during interphase, whereas microhomology-mediated end-joining (MMEJ) has been regarded as a backup mechanism. Through CRISPR-Cas9–based synthetic lethal screens in cancer cells, we identified subunits of the 9-1-1 complex (RAD9A-RAD1-HUS1) and its interacting partner, RHINO, as crucial MMEJ factors. We uncovered an unexpected function for RHINO in restricting MMEJ to mitosis. RHINO accumulates in M phase, undergoes Polo-like kinase 1 (PLK1) phosphorylation, and interacts with polymerase θ (Polθ), enabling its recruitment to DSBs for subsequent repair. Additionally, we provide evidence that MMEJ activity in mitosis repairs persistent DSBs that originate in S phase. Our findings offer insights into the synthetic lethal relationship between the genes *POLQ* and *BRCA1* and *BRAC2* and the synergistic effect of Polθ and poly(ADP-ribose) polymerase (PARP) inhibitors.

Microhomology-mediated end-joining (MMEJ) is an intrinsically mutagenic repair pathway. Nevertheless, it mitigates the harmful effects of double-strand breaks (DSBs) by preventing the accumulation of large-scale DNA rearrangements. Repair by MMEJ is necessary for the survival of cells with compromised homologous recombination (HR) and nonhomologous end-joining (NHEJ) (*1*–*3*). Targeting this pathway has emerged as a promising therapeutic approach for cancer patients with defective HR, including those carrying mutations in the *BRCA1* and *BRCA2* genes (*4*–*6*). MMEJ is characterized by the presence of 2 to 6 base pairs of microhomology, as well as insertions and deletions (indels) that scar the repair sites (*7*). These indels are introduced by DNA polymerase θ (Polθ), which is encoded by the *POLQ* gene. Polθ is a low-fidelity polymerase with a helicase-like activity and plays a central role in MMEJ (*8*, *9*).

The mutational signature associated with MMEJ has been found across different species, and the pathway is conserved from bacteria to humans (*10*). However, its mechanistic basis remains poorly defined. In mammalian cells, studies have demonstrated that after DSB formation, short-range DNA end resection by MRE11 and CtIP exposes flanking microhomologies that promote the annealing of opposite ends of the break (*11*–*13*). When internal homologies are base paired, the resulting single-stranded DNA (ssDNA) flaps are cleaved by APEX2 and FEN1 (*14*–*16*). Annealed intermediates are extended by Polθ (*17*–*19*) and sealed by XRCC1 and LIG3 to complete the end joining (*20*). Polθ also acts on transient "snap-back" substrates that are formed when the overhang of resected DSBs folds back and anneals to itself. Ultimately, Polθ-mediated insertions contribute to the mutagenicity of MMEJ (*19*). Although up-regulated in many cancer types, Polθ is generally low in abundance and must be actively recruited to DSB sites (*21*). Yet the mechanism by which the low-fidelity polymerase is recruited to break sites and the upstream factors that drive MMEJ remain unknown.

MMEJ was initially identified as an inefficient DNA end-joining activity in Ku-deficient *Saccharomyces cerevisiae* (*22*) and has been primarily regarded as a backup pathway that acts when preferred modes of DSB repair are absent (*1*–*3*). However, recent reports suggest that under certain conditions, MMEJ prevails. For instance, MMEJ is the primary repair mechanism for CRISPR-Cas9–induced DSBs in early zebrafish embryos (*23*). In human and mouse cells, MMEJ acts with NHEJ to promote the random integration of foreign DNA into the genome and repair CRISPR-Cas9–induced breaks at particular loci (*24*–*26*). Furthermore, recent evidence suggests that MMEJ plays a role in DSBs during mitosis, where HR and NHEJ are attenuated (*27*–*30*).

Because of the synthetic lethal relationship between MMEJ and HR, Polθ inhibitors are presently under investigation in phase 1 and 2 trials in the clinic as monotherapy and in combination with poly(ADP-ribose) polymerase (PARP) inhibitors (PARPi). Preclinical studies demonstrated that Polθ inhibitors target BRCA-deficient tumors, are synergistic with PARPi, and eliminate a subset of PARPi-resistant tumors (*4*, *6*, *31*). Elucidating the underlying mechanism of MMEJ and its temporal and spatial regulation is critical to understanding when and how cells opt for the mutagenic MMEJ and potentially explain the synthetic lethal interaction between MMEJ and HR.

[1]Molecular Biology Program, Sloan Kettering Institute, Memorial Sloan Kettering Cancer Center, New York, NY, USA. [2]Institute for Quantitative Health Sciences and Engineering, Michigan State University, East Lansing, MI, USA. [3]Department of Obstetrics, Gynecology, and Reproductive Biology, Michigan State University, East Lansing, MI, USA.
*Corresponding author. Email: sfeira@mskcc.org (A.S.); brambata@mskcc.org (A.B.)
†These authors contributed equally to this work.

Results

CRISPR-Cas9 synthetic lethal screen uncovers the full spectrum of MMEJ factors

To identify the full spectrum of MMEJ factors, we conducted a genome-wide CRISPR-based synthetic lethal screen in cells lacking HR and NHEJ [*BRCA2*$^{-/-}$*LIG4*$^{-/-}$*TP53*$^{-/-}$ cells or triple-knockout (TKO) cells]. We hypothesized that because cells that lack these canonical DSB repair pathways are highly dependent on MMEJ for survival, this approach would reveal the full spectrum of potential MMEJ factors (Fig. 1, A to C, and fig. S1, A to D). The synthetic lethal screen identified a set of genes that were preferentially depleted in TKO cells, including hits previously reported to be essential for the survival of *BRCA2*-null cells—such as *FEN1*; *RNaseH2A*, *RNaseH2B*, and *RNaseH2C* (*32*); *CIP2A* (*33*); and *ALC1* (*34*)—as well as known MMEJ factors, including *POLQ*, *HMCES* (*35*), and *APEX2* (*14*–*16*, *36*) (fig. S1, E to G). Notably, we identified members of the 9-1-1 complex (RAD9A-RAD1-HUS1) and its interacting partner RHINO (encoded by *RHNO1*) as essential in TKO cells (Fig. 1, D and E). To confirm the synthetic lethality, we individually targeted subunits of the complex using independent single guide RNAs (sgRNAs). We found that whereas depletion of 9-1-1 and RHINO had little impact on control cells, their loss compromised the survival of cells that lack HR and NHEJ (Fig. 1F and fig. S1, H to J).

RAD9-RAD1-HUS1 (9-1-1) and RHINO are critical MMEJ factors

To directly test whether the 9-1-1 complex and RHINO are required for MMEJ, we investigated the repair of dysfunctional telomeres. The six-subunit shelterin complex protects telomeres from being recognized as DSBs. When shelterin is absent, telomeres become deprotected, and the DNA damage response is activated at chromosome ends (*37*). In cells where telomeres are unprotected and the NHEJ factors Ku70 and Ku80 are absent, MMEJ is the primary repair pathway leading to chromosome end-to-end fusions (*37*) (Fig. 2A). We targeted subunits of the 9-1-1 complex and RHINO in *TRF1/2*$^{\Delta/\Delta}$*Ku80*$^{-/-}$ cells (fig. S2, A and B) and noted a significant reduction in the frequency of MMEJ-dependent telomere fusions (Fig. 2, B and C). Depletion of the 9-1-1 subunits and RHINO in NHEJ-proficient settings had no impact on telomere fusions, suggesting that the activity of 9-1-1 and RHINO is specific to MMEJ (Fig. 2D). Despite the reduced MMEJ activity, the absence of 9-1-1 and RHINO did not prevent the accumulation of 53BP1 at shelterin-free telomeres (fig. S2, C and D). This implies that the canonical role of the 9-1-1 complex in activating DNA damage signaling through ATR kinase (*38*) does not completely account for its function in MMEJ. In an orthogonal approach, we measured MMEJ activities at a break induced by the endonuclease

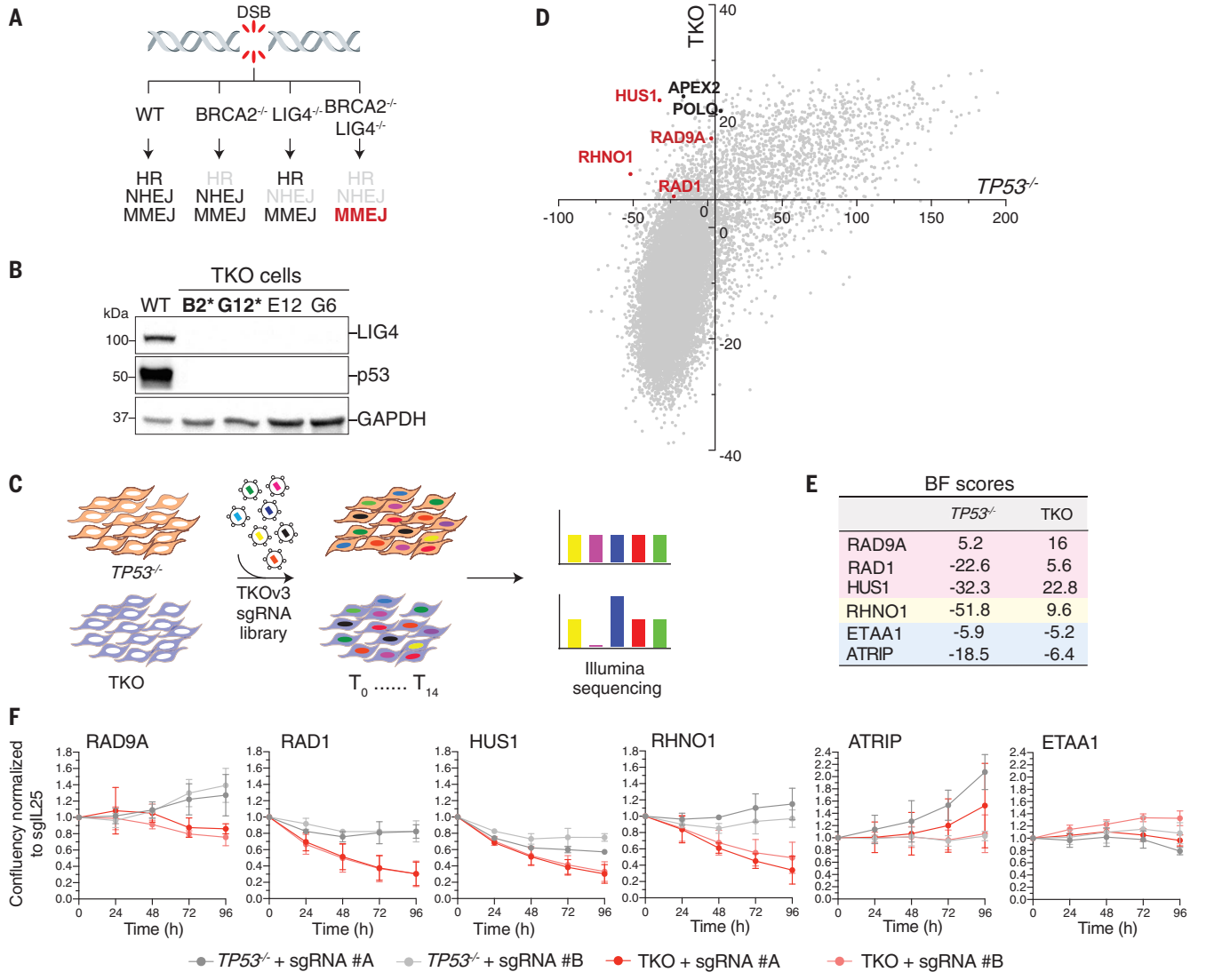

Fig. 1. A genome-wide CRISPR-Cas9 screen uncovers an essential function for 9-1-1 and RHNO1 in cells that lack BRCA2 and LIG4. (**A**) Schematic of the three major DSB repair pathways in mammalian cells. WT, wild type. (**B**) Western blot analysis of LIG4 and p53 in clonally derived *BRCA2*$^{-/-}$*LIG4*$^{-/-}$*TP53*$^{-/-}$ DLD1 cells (TKO). The asterisk indicates clones used in the screen. GAPDH, glyceraldehyde phosphate dehydrogenase. (**C**) Schematic of the dropout CRISPR-Cas9 screen to identify synthetic lethal interactions. (**D**) Genome-wide CRISPR-Cas9 screen result in TKO cells. Genes with a Bayes factor (BF) score >5 (intersection of *x* and *y* axes) were considered essential. (**E**) BF scores for the indicated genes. (**F**) Growth curve of TKO and *TP53*$^{-/-}$ cells treated with the indicated sgRNAs. Data are mean ± SD of three independent experiments normalized to time point zero (1 day after seeding) and a control sgRNA (sgIL25).

I-SceI using the traffic light reporter (TLR) system (*39*) (fig. S2E). Findings based on the fluorescent DSB reporter corroborated the results derived from the telomere fusion assay and are consistent with Repair-seq (*40*), which demonstrated a correlation between *POLQ* and the 9-1-1 complex as well as the Rad17-RFC clamp loader (Fig. 2, B and D, and figs. S1G and S2, E to I).

A noncanonical function for 9-1-1 and RHINO in MMEJ

9-1-1 is a heterotrimeric complex loaded onto 5′ ends of resected DNA and ssDNA gaps in response to replication stress (*38*). Its interaction with RHINO induces DNA damage signaling by ATR (*41*, *42*). ATR is also activated by ETAA1 and its interacting partner ATRIP (*43*, *44*). Notably, in the synthetic lethal screen, *ATRIP* and *ETAA1* did not emerge as potential hits (Fig. 1E), and CRISPR-Cas9–mediated deletion of these genes did not result in growth defects in TKO cells (Fig. 1F and fig. S1, K to N). Moreover, whereas the loss of ATRIP had a minor impact on telomere fusions, ETAA1 depletion did not impair MMEJ (fig. S3, A to E). By contrast, depletion of 9-1-1, RHINO, and Polθ significantly reduced telomere fusion events (Fig. 2, B and C, and fig. S3, A to E). These findings suggest that the established role of 9-1-1 and RHINO in ATR signaling does not entirely explain their function in MMEJ.

The 9-1-1 subunits assemble into a ring-shaped complex that structurally resembles proliferating cell nuclear antigen (PCNA), which recruits DNA polymerases to the replisome (*45*). We speculated that 9-1-1 and RHINO might facilitate MMEJ by interacting with and recruiting Polθ to break sites. We performed coimmunoprecipitation (co-IP) experiments in human embryonic kidney 293T (HEK293T) cells coexpressing 9-1-1 proteins, RHINO, and Polθ. Although we could not detect an interaction between Polθ and any of the subunits of the 9-1-1 complex (fig. S3F), we observed an interaction between Polθ and RHINO, independent of DNA damage (Fig. 2E). In addition, using purified proteins, we

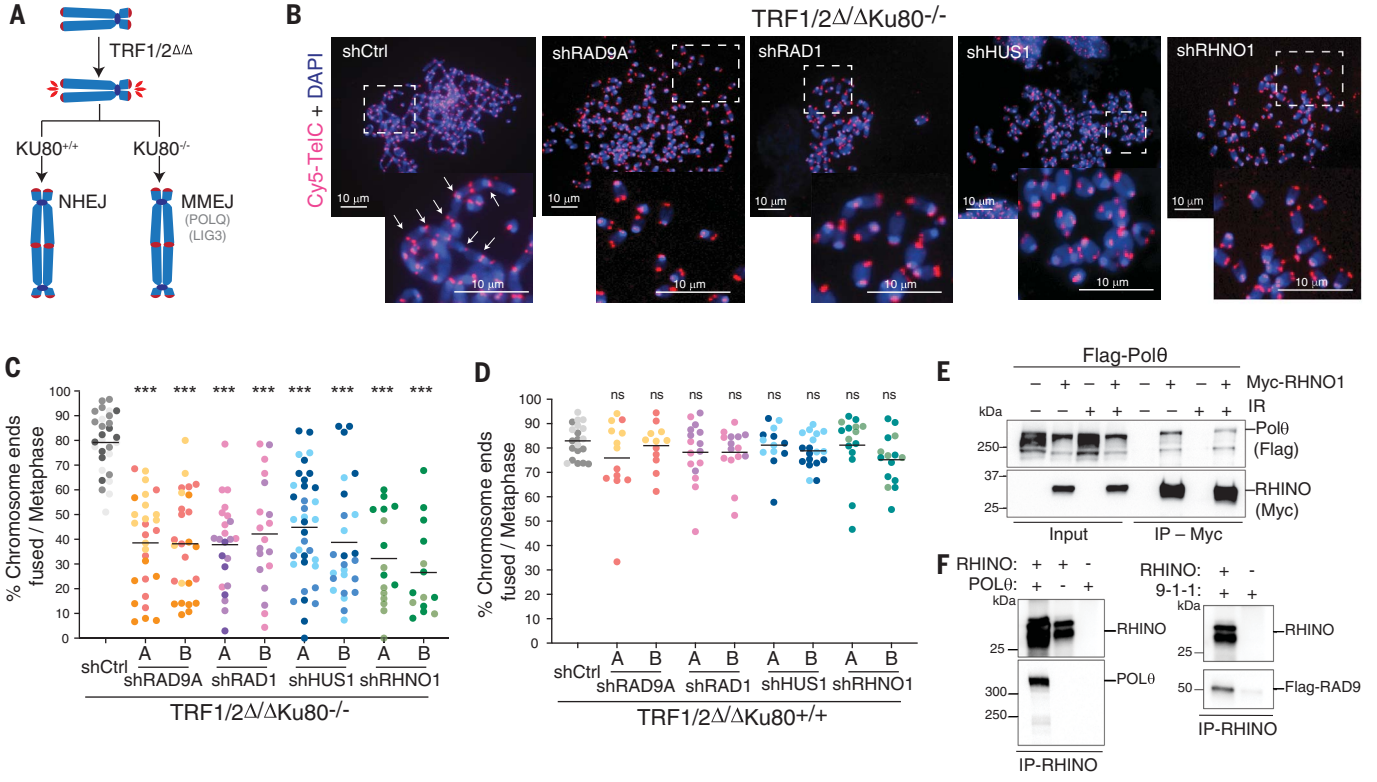

Fig. 2. A noncanonical function for 9-1-1–RHINO in MMEJ. (**A**) Schematic of the shelterin-free assay (*37*) to monitor MMEJ frequency at deprotected telomeres. (**B**) Representative images of metaphase spreads from *TRF1/2*$^{\Delta/\Delta}$*Ku80*$^{-/-}$ cells depleted for the subunits of the 9-1-1 complex and *RHNO1* with two independent short hairpin RNAs (shRNAs). Telomeres are marked by fluorescence in situ hybridization (FISH) using a Cy5-[CCCTAA]3 peptide nucleic acid (PNA) probe (red), and chromosomes are counterstained with 4′,6-diamidino-2-phenylindole (DAPI) (blue). White arrows indicate examples of telomeric fusions in the control (shCtrl) sample. The dashed rectangles highlight the magnification in (C). (**C**) Quantification of telomeric fusions mediated by MMEJ as shown in (B). The colors used indicate independent experiments. The black line represents the mean. (**D**) Quantification of telomere fusions by NHEJ in TRF1/2$^{\Delta/\Delta}$Ku80$^{+/+}$ cells. Data in (C) and (D) are the mean of at least two independent experiments. Significance was determined by one-way analysis of variance (ANOVA) (***$p < 0.001$; ns, not significant). (**E**) Co-IP experiment depicting the Polθ and RHINO interaction in whole-cell extracts from HEK293T cells cotransfected with plasmids expressing Flag-Polθ and RHINO-MYC. Co-IPs were performed in cells treated with ionizing radiation [+IR, 20 gray (Gy)] and control cells. (**F**) Co-IP experiments showing the interactions of Polθ-RHINO and 9-1-1–RHINO with purified proteins. Polθ was purified from HEK293T cells, RHINO from *Escherichia coli*, and 9-1-1 from *S. cerevisiae*.

found that RHINO bound full-length Polθ in vitro (Fig. 2F and fig. S3G).

RHINO is predominantly expressed in mitosis, and its phosphorylation by PLK1 stimulates the interaction with Polθ

To gain better insight into the function of RHINO, we sought to determine its genetic interactors. We carried out synthetic lethal screens in three clonally derived *RHNO1*$^{-/-}$ cell lines and the parental *RHNO1*$^{+/+}$ cells (Fig. 3A and fig. S4, A to G). Pathway analysis of top genes essential in *RHNO1*$^{-/-}$ cells revealed enrichment in several pathways related to mitosis (Fig. 3B), including cyclin-dependent kinase *CDK1*, members of the ESCRT complex, spindle checkpoint proteins, and the kinetochore factor *ZWILCH* (Fig. 3A and figs. S4, F and G, and S5, A and B). Independently, we analyzed the genetic dependencies in DepMap (*46*) and found that *RHNO1* correlated with *CIP2A*, *MDC1*, and *TOPBP1*, which form a complex that tethers mitotic DSBs together (*33*, *47*, *48*). DepMap analysis also uncovered a correlation between the essentiality scores of *POLQ*, *CIP2A*, and *RHNO1* (Fig. 3C).

The results from the synthetic lethal screen and DepMap analysis underscored a previously unrecognized role for RHINO in repairing DNA damage in mitosis. This observation was substantiated by the accumulation of large RHINO foci in cells arrested in M phase (Fig. 3, D and E, and fig. S5, C and D). Furthermore, Western blot analysis of samples collected at different cell cycle stages revealed that RHINO accumulated in mitosis and was rapidly degraded upon mitotic exit (Fig. 3F and fig. S6, A to D). By contrast, subunits of the 9-1-1 complex were expressed throughout all cell cycle stages (fig. S6, C to E). As anticipated by the strict expression of RHINO, Polθ interacted with Flag-RHINO, specifically in mitosis (Fig. 3G). Coincident with its stabilization, RHINO was phosphorylated in mitosis (fig. S6F).

RHINO contains two recognition sequences for the anaphase-promoting complex (APC/C), namely the Ken-box and D-box domains (*49*) (Fig. 3H). Expression of RHINO-ΔDK, which carries deletions in both degrons, resulted in RHINO stabilization beyond mitosis (Fig. 3I). Furthermore, the overexpression of the APC/C adaptor protein Cdh1, but not Cdc20, led to RHINO depletion, suggesting that its degradation is a late event in mitosis (fig. S6G) (*49*). Although RHINO-ΔDK remained stable during interphase, it only interacted with Polθ in mitosis (fig. S6H). Based on this observation, we explored whether the interaction between RHINO and Polθ could be stimulated by phosphorylation. We found that inhibiting the major mitotic kinase CDK1, and to a lesser extent Polo family kinase PLK1, hindered RHINO

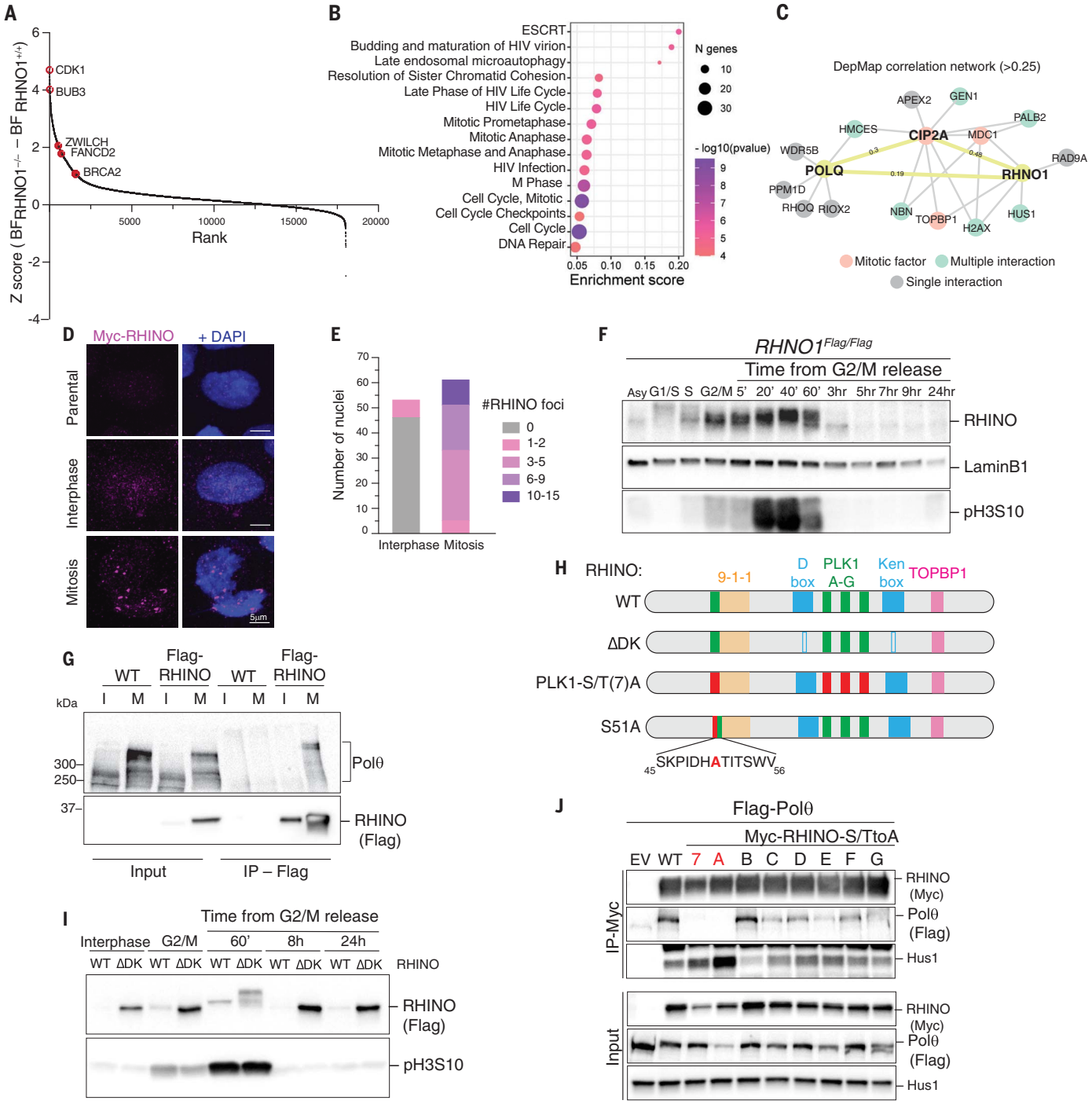

Fig. 3. RHINO is predominantly expressed in mitosis. (**A**) Results from the CRISPR-Cas9 dropout screen in *RHNO1*$^{-/-}$ and isogenic *RHNO1*$^{+/+}$ cells. Ranked *z*-scores of the difference in BF scores. (**B**) Reactome pathway overrepresentation analysis of synthetic lethal genes with *RHNO1*$^{-/-}$. The fold enrichment of each pathway is plotted on the *x* axis. The number of genes associated with each pathway is indicated by the size of the circle, and the color shade indicates the *p* value. (**C**) Network analysis for *POLQ* and *RHNO1* based on Pearson's correlation of dependency scores derived from DepMap. (**D**) Representative immunofluorescence images of RHINO in interphase and mitotic cells. (**E**) Quantification of RHINO foci from (D). (**F**) Western blot analysis of endogenous RHINO at different stages of the cell cycle. Extracts from *RHNO1*$^{Flag/Flag}$ cells at the indicated time points. pH3S10 antibody was used as a mitotic marker, and Lamin B1 was used as a loading control. (**G**) Control cells and cells expressing RHINO-MYC-Flag were synchronized in mitosis and subjected to anti-Flag immunoprecipitation followed by Western blot for endogenous Polθ. I, interphase; M, mitosis. (**H**) Schematic of RHINO protein highlighting the binding domains for 9-1-1 and TOPBP1, D and Ken boxes (ΔDK), and the PLK1 phosphorylation sites [PLK1(S/T)7A and S51A]. RHINO PLK1(S/T)A harbors alanine mutations in all seven predicted PLK1 sites. RHINO S51A harbors a single mutation of serine-51 (conserved among primates and rodents) to alanine. (**I**) Western blot analysis of RHINO and RHINOΔDK during the cell cycle. (**J**) Co-IP experiments in HEK293T cells cotransfected with plasmids expressing FLAG-Polθ and RHINO-MYC mutants. RHINO mutants with a single serine or threonine mutation to alanine are labeled A through G. EV, empty vector.

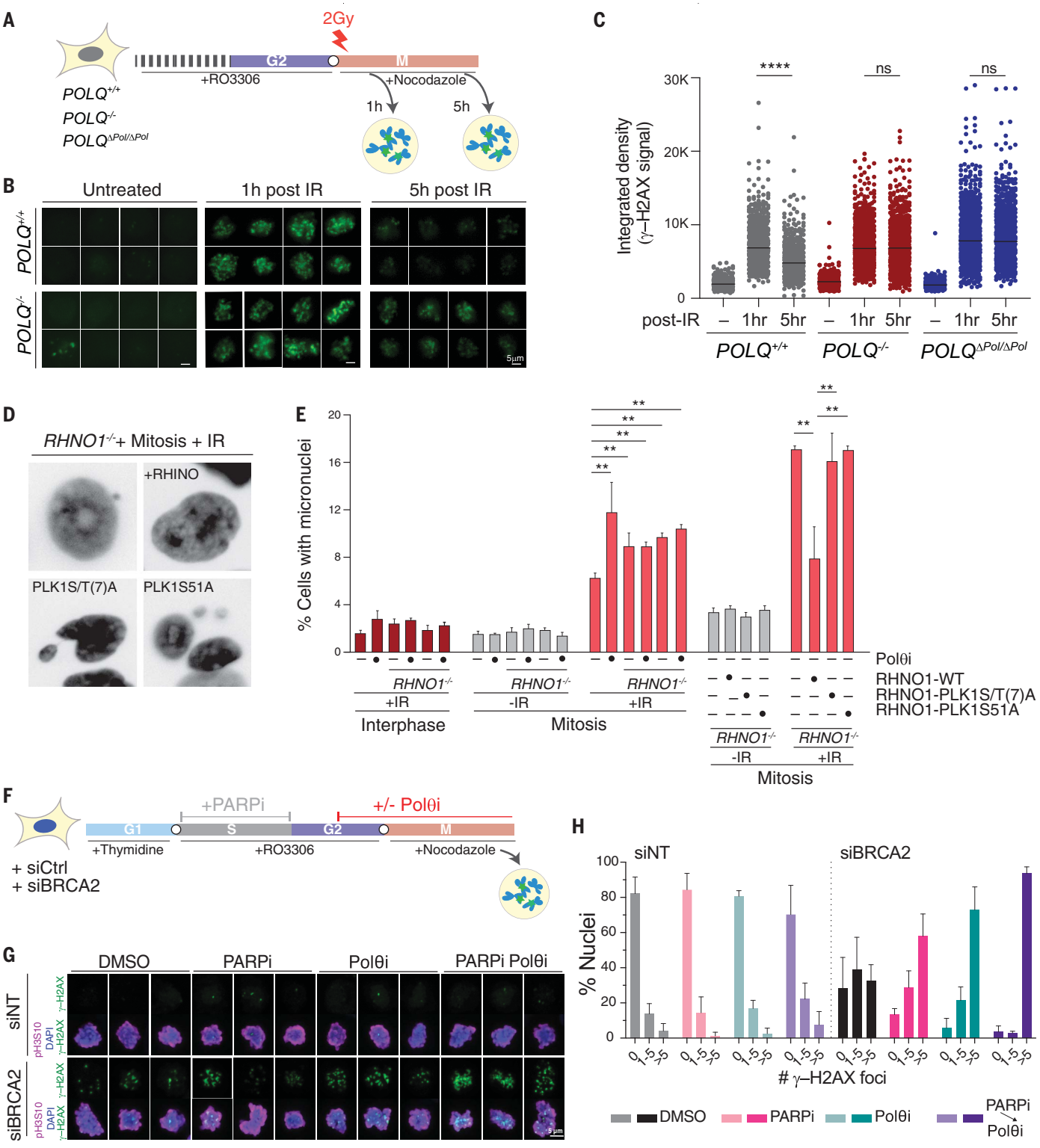

Fig. 4. MMEJ is the predominant DSB repair pathway during mitosis. (**A**) Schematic of the experimental design to detect MMEJ in mitosis that was used to obtain the results shown in (B) and (C). (**B**) Representative images of γ-H2AX in cells treated as described in (A). (**C**) Quantification of γ-H2AX intensity in mitotic cells with the indicated genotype. Black horizontal lines indicate means (n > 450 cells; paired t test; ****p < 0.0001; ns, not significant). (**D**) Representative images of micronuclei in cells with the indicated treatment and genotype. (**E**) Quantification of micronuclei formation after irradiation during interphase and mitosis as shown in (D). Bars represent the mean ± SD of three independent experiments (n > 250 cells; paired t test; **p < 0.01). (**F**) Schematic of the experimental pipeline for (G) and (H). (**G**) Representative immunofluorescence images of mitotic cells treated as described in (F) and stained with anti–γ-H2AX. pH3S10 is used to mark mitotic chromosomes. DNA is stained with DAPI. DMSO, dimethyl sulfoxide. (**H**) Quantification of γ-H2AX foci in mitotic cells with the indicated treatment. Bars represent the mean ± SD of three independent experiments (n > 50 cells).

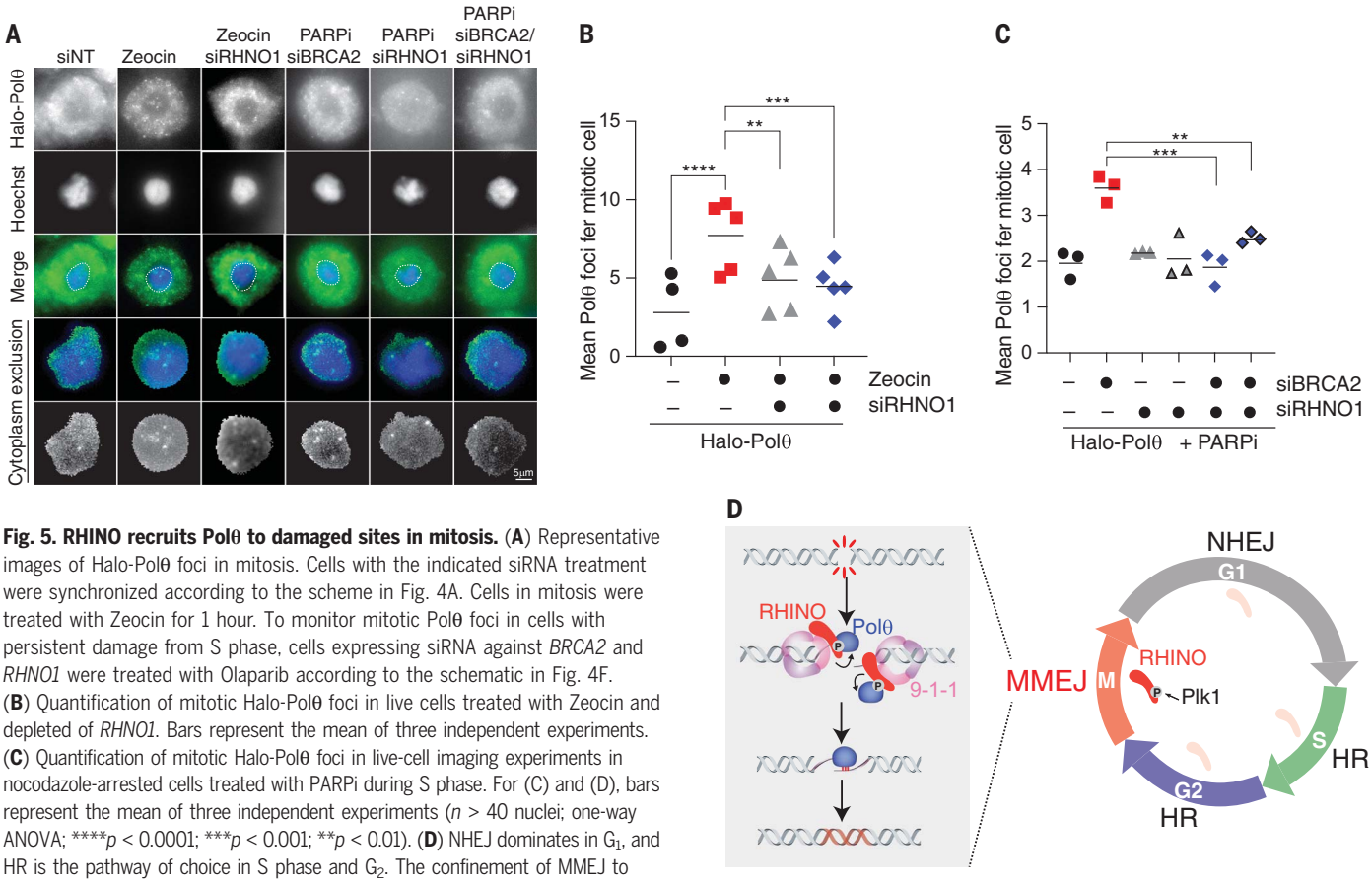

Fig. 5. RHINO recruits Polθ to damaged sites in mitosis. (**A**) Representative images of Halo-Polθ foci in mitosis. Cells with the indicated siRNA treatment were synchronized according to the scheme in Fig. 4A. Cells in mitosis were treated with Zeocin for 1 hour. To monitor mitotic Polθ foci in cells with persistent damage from S phase, cells expressing siRNA against *BRCA2* and *RHNO1* were treated with Olaparib according to the schematic in Fig. 4F. (**B**) Quantification of mitotic Halo-Polθ foci in live cells treated with Zeocin and depleted of *RHNO1*. Bars represent the mean of three independent experiments. (**C**) Quantification of mitotic Halo-Polθ foci in live-cell imaging experiments in nocodazole-arrested cells treated with PARPi during S phase. For (C) and (D), bars represent the mean of three independent experiments ($n > 40$ nuclei; one-way ANOVA; ****$p < 0.0001$; ***$p < 0.001$; **$p < 0.01$). (**D**) NHEJ dominates in G_1, and HR is the pathway of choice in S phase and G_2. The confinement of MMEJ to mitosis occurs because of the accumulation of RHINO during M phase, PLK1 phosphorylation, and the recruitment of Polθ to DNA breaks.

phosphorylation (fig. S6, I to K). RHINO contains seven Ser-Pro and/or Thr-Pro motifs that are susceptible to CDK1 targeting and seven Ser and/or Thr residues embedded within the consensus motif of PLK1. Using Phospho-Tag gels, we determined that RHINO phosphorylation was altered in the context of RHINO-PLK1S/T(7)A and abrogated in the RHINO-CDK1S/T(7)A allele (fig. S6, J and K). These findings are consistent with CDK1 phosphorylation being a priming event for subsequent PLK1 phosphorylation of RHINO. Such sequential modification is commonly observed in PLK1 targets, including BUB1, BUBR1, and CLASP2 (*50*–*52*). Notably, co-IP analysis showed that RHINO-PLK1S/T(7)A failed to bind Polθ (Fig. 3J and fig. S6L). Furthermore, by individually mutating seven PLK1 sites, we identified a single phosphorylation residue on RHINO (S51) that, when mutated to alanine, exhibited a reduced interaction with Polθ (Fig. 3J and fig. S6L).

MMEJ is a dominant DSB repair pathway in mitosis

Unresolved damage during S phase and G_2 of the cell cycle can be carried over to mitosis. However, it is well established that NHEJ and HR are repressed during M phase (*53*, *54*). Recently, a tethering complex comprising MDC1-CIP2A-TOPBP1 was reported to hold broken mitotic DNA ends together until cells progress into the next G_1 (*33*, *47*, *48*). Multiple studies implicated Polθ activity in repairing DNA damage in mitosis (*27*–*30*). An investigation using *Xenopus* egg extract showed that entry into mitosis before the completion of DNA replication leads to complex rearrangements driven by Polθ (*29*). In addition, Polθ was linked to the formation of sister chromatid exchanges (SCEs) as under-replicated DNA is transferred into mitosis (*30*). Last, it was shown that MMEJ activity is delayed until mitosis in cells that lack BRCA2, where Rad52 blocked Polθ activity in G_2 (*27*). We conducted individual and combined depletion of RHINO and CIP2A in *BRCA2*$^{-/-}$ cells and observed an additive effect on growth, suggesting that RHINO-mediated MMEJ is independent of mitotic tethering of DNA breaks (fig. S7, A and B). Consistent with the involvement of Polθ in mitotic repair, *POLQ*$^{-/-}$ cells were more sensitive to DNA damage when treated with ionizing radiation in mitosis relative to interphase (fig. S7, C and D).

Given the critical function of RHINO in MMEJ, its enrichment in mitosis, and its interaction with Polθ, we hypothesized that RHINO could promote mitotic MMEJ by facilitating Polθ recruitment to condensed chromosomes. To assay MMEJ activity in mitosis, we synchronized *POLQ*$^{-/-}$ and *POLQ*$^{+/+}$ cells at the G_2-M boundary using a CDK1 inhibitor. We then released cells into M phase in the presence of nocodazole, which prevented mitotic exit. We irradiated cells 30 min after release from CDK1 inhibition and monitored the dissolution of phosphorylated γ-H2AX (Fig. 4A). Wild-type cells accumulated maximal γ-H2AX 1 hour after irradiation, which significantly decreased after 5 hours (Fig. 4, B and C, and fig. S7E). As a control, we showed a similar resolution of γ-H2AX foci in *LIG4*$^{-/-}$ cells relative to wild-type cells, confirming the lack of NHEJ activity in mitosis (fig. S7F). By contrast, *POLQ*$^{-/-}$ cells and ones carrying inactivating mutations in the polymerase domain of Polθ (*POLQ*$^{\Delta Pol/\Delta Pol}$) failed to resolve γ-H2AX foci (Fig. 4, B and C, and fig. S7F). Furthermore, treatment of cells with Polθ inhibitor (Polθi-RP6685) (*31*) during mitosis, but not interphase, led to the persistence of γ-H2AX foci after

irradiation (fig. S7, G and H). Similarly, the absence of RHINO prevented the resolution of γ-H2AX after radiation treatment (fig. S7I). Last, we corroborated the essentiality of MMEJ activity in mitotic DSB repair by using the inducible restriction enzyme AsiSI (*55*) and observed a defect in γ-H2AX resolution in cells treated with Polθ inhibitor (fig. S7, J to L).

Unrepaired mitotic DSBs are especially toxic because they can result in lagging chromosome fragments that accumulate in micronuclei and trigger chromothripsis (*56*). We tested whether MMEJ activity prevents micronuclei formation after irradiation of cells in mitosis. Polθ inhibition and RHINO deletion significantly increased micronuclei formation (Fig. 4, D and E). Blocking Polθ in *RHNO1*$^{-/-}$ cells had no additive effect on the accumulation of micronuclei, suggesting that the two factors are epistatic (Fig. 4E). Furthermore, we expressed RHINO-WT, RHINO-PLK1-S/T(7)A, and RHINO-S51A alleles in *RHNO1*$^{-/-}$ cells and found that both mutants failed to rescue micronuclei formation after mitotic irradiation (Fig. 4, D and E). Similarly, *RHNO*$^{-/-}$ cells and ones complemented with the RHINO-S51A allele failed to resolve mitotic γ-H2AX accumulation (fig. S7I). In conclusion, our findings implicate the RHINO-Polθ interaction in stimulating MMEJ during mitosis.

Mitotic MMEJ resolves DNA breaks that originate in S phase in BRCA2 *mutant cells*

We next tested whether the activity of RHINO and Polθ in mitosis was necessary to repair DNA lesions that arise in S phase and G_2 but persist into M phase (Fig. 4F). We used small interfering RNA (siRNA) against *BRCA2* (fig. S8A) to block repair by HR and induced DNA damage in S phase by incubating cells with PARPi (Olaparib) (*57*). As cells progressed beyond S phase, we withdrew PARPi from the culture medium. Toward the end of G_2, we added Polθi, which was continuously present as cells entered mitosis. To prevent mitotic exit, cells were treated with nocodazole before fixing them for subsequent analysis for γ-H2AX (Fig. 4, F to H, and fig. S8B). We observed a baseline increase in γ-H2AX foci in mitotic cells treated with si*BRCA2* compared with those treated with control siRNA. As expected, the levels of γ-H2AX were more elevated in cells treated with either Olaparib in S phase or Polθ inhibitor in G_2 and M phase. Cells treated with PARP inhibitor in S phase and Polθ inhibitor in G_2-M displayed a synergistic increase in γ-H2AX accumulation (Fig. 4, F to H). Furthermore, this synergy was observed when the polymerase was inhibited in mitosis but not during S phase (fig. S8, C to E). To further substantiate the role of mitotic MMEJ in repairing unresolved S phase damage, we treated *RHNO1*$^{-/-}$ cells with siRNA against *BRCA2* and observed a similar synergistic effect with PARPi treatment (fig. S8F).

RHINO recruits Polθ to DSB sites in mitosis

Having established a role for MMEJ in repairing breaks in mitosis, we next investigated whether RHINO recruits Polθ to damage sites to facilitate mitotic repair. We used a two-step CRISPR-Cas9 targeting strategy to establish cells where *POLQ* was endogenously tagged with Halo at the N terminus (fig. S9, A to C). We treated *POLQ*$^{Halo/Halo}$ cells with a Halo-tag ligand (JFX650) and traced Polθ single particles using live-cell imaging in interphase and mitosis (fig. S9D and movies S1 and S2). To test whether RHINO acts upstream of Polθ, we arrested *POLQ*$^{Halo/Halo}$ cells treated with si*RHNO1* at the G_2-M boundary by CDK1 inhibition and released them into mitosis. Treatment of mitotic cells with Zeocin resulted in large and static Polθ foci. Polθ foci were significantly reduced upon *RHNO1* depletion but not affected by MDC1 loss and ATR inhibition (Fig. 5, A and B, and figs. S9, E to I, and S10, A to E). Last, we investigated the static Polθ foci in the context of unresolved S phase damage that persisted into mitosis. We treated *BRCA2*-depleted *POLQ*$^{Halo/Halo}$ cells with PARPi in S phase and showed that Polθ dynamics and colocalization with replication protein A (RPA) were largely unchanged when monitored in S phase (fig. S11A). However, this same treatment led to the accumulation of static Polθ foci in mitosis (Fig. 5, A to C, and figs. S9E and S11, B and C). These findings provide further evidence for the role of RHINO in recruiting Polθ to break sites during mitosis.

Discussion

NHEJ predominates in G_1, whereas HR is preferred for repairing DSBs in S phase and G_2 (*58*–*60*). In this work, we demonstrate that in mitosis, where both HR and NHEJ are repressed (*53*, *54*), MMEJ is the sole DSB repair pathway. MMEJ activity in M phase is driven by the accumulation of RHINO to promote Polθ recruitment to damage sites (Fig. 5D). The decoupling of DNA repair pathways during different stages of the cell cycle has implications for maintaining genome stability. Mitotic MMEJ may have evolved as a fail-safe mechanism that operates on highly condensed chromosomes and ensures that cells do not commit to cellular division with unrepaired lesions that trigger genome instability. Conversely, suppression of MMEJ in G_1 and S-G_2 could protect genomes from the intrinsic mutagenic potential of this pathway.

RHINO was previously identified as a 9-1-1–interacting protein that is required for activating ATR signaling (*41*, *42*) but now emerges as a critical factor that promotes MMEJ during mitosis. We show that RHINO, but not 9-1-1 complex members, is greatly stabilized in mitosis and degraded by the APC/C complex upon mitotic exit (Fig. 3, H and I). Based on our data, we propose that PLK1-dependent phosphorylation of RHINO facilitates its interaction with Polθ to stimulate MMEJ. A recent study has also identified PLK1 phosphorylation sites on Polθ that are critical for mitotic MMEJ (*61*). Furthermore, it has been established that the CDK1-PLK1 signaling axis attenuates NHEJ and HR by phosphorylating and inhibiting 53BP1 and BRCA2, respectively (*62*–*64*). These studies highlight the multifaceted role of PLK1 in controlling repair pathway choice in mitosis.

RHINO is highly unstructured and interacts with RAD1 and TOPBP1 through distinct domains (*41*, *42*). Unrepaired S phase damage may be marked by 9-1-1 through mitosis, where RHINO accumulates. Tethering RHINO to the 9-1-1 complex in M phase would subsequently lead to Polθ recruitment to break sites, thereby enabling MMEJ. RHINO-TOPBP1 interaction in mitosis could stabilize RHINO at break sites and form a complex that recruits Polθ. Further structural studies could provide a deeper insight into 9-1-1–RHINO–Polθ–TOPBP1 complex formation and probe the impact of PLK1 phosphorylation.

Our study does not rule out a role for Polθ in filling ssDNA gaps after replication, nor do we exclude the possibility of RHINO-independent MMEJ activity during S phase (*65*–*68*). However, our findings provide evidence suggesting that robust MMEJ activity in mitosis accounts for the synthetic lethal interaction between Polθ and BRCA2. Uncoupling DNA repair activities during different cell cycle stages provides a rationale for the reported synergy of Polθ inhibitors with PARPi and potentially other antineoplastic therapies that induce DNA damage during S phase (*4*, *6*).

REFERENCES AND NOTES

1. P. A. Mateos-Gomez *et al*., *Nature* **518**, 254–257 (2015).
2. R. Ceccaldi *et al*., *Nature* **518**, 258–262 (2015).
3. D. W. Wyatt *et al*., *Mol. Cell* **63**, 662–673 (2016).
4. D. Zatreanu *et al*., *Nat. Commun.* **12**, 3636 (2021).
5. A. Schrempf, J. Slyskova, J. I. Loizou, *Trends Cancer* **7**, 98–111 (2021).
6. J. Zhou *et al*., *Nat. Cancer* **2**, 598–610 (2021).
7. A. Sfeir, L. S. Symington, *Trends Biochem. Sci.* **40**, 701–714 (2015).
8. S. J. Black *et al*., *Nat. Commun.* **10**, 4423 (2019).
9. P. A. Mateos-Gomez *et al*., *Nat. Struct. Mol. Biol.* **24**, 1116–1123 (2017).
10. D. A. Ramsden, J. Carvajal-Garcia, G. P. Gupta, *Nat. Rev. Mol. Cell Biol.* **23**, 125–140 (2022).
11. L. N. Truong *et al*., *Proc. Natl. Acad. Sci. U.S.A.* **110**, 7720–7725 (2013).
12. A. Xie, A. Kwok, R. Scully, *Nat. Struct. Mol. Biol.* **16**, 814–818 (2009).
13. M. Lee-Theilen, A. J. Matthews, D. Kelly, S. Zheng, J. Chaudhuri, *Nat. Struct. Mol. Biol.* **18**, 75–79 (2011).
14. H. Fleury *et al*., *Mol. Cell* **83**, 1429–1445.e8 (2023).
15. S. Sharma *et al*., *Cell Death Dis.* **6**, e1697 (2015).
16. K. E. Mengwasser *et al*., *Mol. Cell* **73**, 885–899.e6 (2019).
17. S. H. Chan, A. M. Yu, M. McVey, *PLOS Genet.* **6**, e1001005 (2010).
18. M. E. Arana, M. Seki, R. D. Wood, I. B. Rogozin, T. A. Kunkel, *Nucleic Acids Res.* **36**, 3847–3856 (2008).
19. T. Kent, P. A. Mateos-Gomez, A. Sfeir, R. T. Pomerantz, *eLife* **5**, e13740 (2016).
20. M. Audebert, B. Salles, P. Calsou, *J. Biol. Chem.* **279**, 55117–55126 (2004).

21. M. Seki, F. Marini, R. D. Wood, *Nucleic Acids Res.* **31**, 6117–6126 (2003).
22. S. J. Boulton, S. P. Jackson, *EMBO J.* **15**, 5093–5103 (1996).
23. S. B. Thyme, A. F. Schier, *Cell Rep.* **15**, 1611–1613 (2016).
24. J. Schimmel, H. Kool, R. van Schendel, M. Tijsterman, *EMBO J.* **36**, 3634–3649 (2017).
25. S. Saito, R. Maeda, N. Adachi, *Nat. Commun.* **8**, 16112 (2017).
26. B. Corneo *et al*., *Nature* **449**, 483–486 (2007).
27. M. Llorens-Agost *et al*., *Nat. Cell Biol.* **23**, 1095–1104 (2021).
28. H. Wang *et al*., *Nucleic Acids Res.* **46**, 10724–10739 (2018).
29. L. Deng *et al*., *Mol. Cell* **73**, 915–929.e6 (2019).
30. A. M. Heijink *et al*., *Nat. Commun.* **13**, 6722 (2022).
31. M. Bubenik *et al*., *J. Med. Chem.* **65**, 13198–13215 (2022).
32. M. Zimmermann *et al*., *Nature* **559**, 285–289 (2018).
33. S. Adam *et al*., *Nat. Cancer* **2**, 1357–1371 (2021).
34. P. Verma *et al*., *Nat. Cell Biol.* **23**, 160–171 (2021).
35. V. Shukla *et al*., *Mol. Cell* **77**, 1154 (2020).
36. A. Álvarez-Quilón *et al*., *Mol. Cell* **78**, 1152–1165.e8 (2020).
37. A. Sfeir, T. de Lange, *Science* **336**, 593–597 (2012).
38. J. A. Melo, J. Cohen, D. P. Toczyski, *Genes Dev.* **15**, 2809–2821 (2001).
39. M. T. Certo *et al*., *Nat. Methods* **8**, 671–676 (2011).
40. J. A. Hussmann *et al*., *Cell* **184**, 5653–5669.e25 (2021).
41. C. Cotta-Ramusino *et al*., *Science* **332**, 1313–1317 (2011).
42. L. A. Lindsey-Boltz, M. G. Kemp, C. Capp, A. Sancar, *Cell Cycle* **14**, 99–108 (2015).
43. T. E. Bass *et al*., *Nat. Cell Biol.* **18**, 1185–1195 (2016).
44. D. A. Mordes, G. G. Glick, R. Zhao, D. Cortez, *Genes Dev.* **22**, 1478–1489 (2008).
45. C. S. Eichinger, S. Jentsch, *Trends Biochem. Sci.* **36**, 563–568 (2011).
46. Broad Institute, DepMap Portal (2021); https://depmap.org/portal/.
47. P. A. Leimbacher *et al*., *Mol. Cell* **74**, 571–583.e8 (2019).
48. M. De Marco Zompit *et al*., *Nat. Commun.* **13**, 4143 (2022).
49. M. Sullivan, D. O. Morgan, *Nat. Rev. Mol. Cell Biol.* **8**, 894–903 (2007).
50. P. Singh *et al*., *Mol. Cell* **81**, 67–87.e9 (2021).
51. A. E. Elia *et al*., *Cell* **115**, 83–95 (2003).
52. A. R. Maia *et al*., *J. Cell Biol.* **199**, 285–301 (2012).
53. A. N. Blackford, M. Stucki, *Trends Biochem. Sci.* **45**, 321–331 (2020).
54. R. E. Zirkle, W. Bloom, *Science* **117**, 487–493 (1953).
55. J. S. Iacovoni *et al*., *EMBO J.* **29**, 1446–1457 (2010).
56. C. Z. Zhang *et al*., *Nature* **522**, 179–184 (2015).
57. J. Murai *et al*., *Cancer Res.* **72**, 5588–5599 (2012).
58. A. Beucher *et al*., *EMBO J.* **28**, 3413–3427 (2009).
59. K. Karanam, R. Kafri, A. Loewer, G. Lahav, *Mol. Cell* **47**, 320–329 (2012).
60. K. Nakamura *et al*., *Nat. Cell Biol.* **21**, 311–318 (2019).
61. C. Gelot *et al*., bioRxiv 2023.03.17.533134 [Preprint] (2023); https://doi.org/10.1101/2023.03.17.533134
62. F. Esashi *et al*., *Nature* **434**, 598–604 (2005).
63. D. H. Lee *et al*., *Mol. Cell* **54**, 512–525 (2014).
64. A. Orthwein *et al*., *Science* **344**, 189–193 (2014).
65. S. F. Roerink, R. van Schendel, M. Tijsterman, *Genome Res.* **24**, 954–962 (2014).
66. O. Belan *et al*., *Mol. Cell* **82**, 4664–4680.e9 (2022).
67. A. Schrempf *et al*., *Cell Rep.* **41**, 111716 (2022).
68. A. Mann *et al*., *Mol. Cell* **82**, 4218–4231.e8 (2022).

ACKNOWLEDGMENTS

We thank D. Durocher, R. Weiss, and R. Greenberg for providing critical reagents for this study. We thank D. Remus for providing 9-1-1 proteins and assisting with in vitro assays. S. Morris and M.-C. Mathieu from Repare Therapeutics generously provided reagents. We thank E. Lazzerini-Denchi and members of the Sfeir lab for commenting on the manuscript. We thank S. Deng, T. Lieber, Y. Fu, M. Selvaraj, and H. Shah for their experimental assistance. **Funding:** This work was supported by the following grants: National Institutes of Health (NIH) grant R01CA229161 (A.S.), NIH grant DP2CA195767-01 (A.S.), a Pershing Square-Sohn Cancer Foundation grant (A.S.), a V-foundation grant (A.S.), a New York Stem Cell Foundation training grant (A.B.), NIH grant F32GM139292 (J.H.), and NIH grant DP2GM142307 (J.C.S.). **Author contributions:** Conceptualization: A.B., A.S.; Methodology: A.B., O.S., S.P., J.H., M.K., A.S.; Investigation: A.B., O.S., S.P., J.H., M.K., A.S.; Funding acquisition: J.C.S., A.S.; Project administration: A.S.; Supervision: A.S.; Writing – original draft: A.B., A.S.; Writing – review and editing: A.B., O.S., S.P., J.H., M.K., J.C.S., A.S. **Competing interests:** A.S. is a cofounder, consultant, and shareholder of Repare Therapeutics. All other authors have no competing interests. **Data and materials availability:** All data are available in the main text and supplementary materials. All material will be shared upon request.

SUPPLEMENTARY MATERIALS

science.org/doi/10.1126/science.adh3694
Materials and Methods
Figs. S1 to S11
Tables S1 and S2
References (*69*–*75*)
MDAR Reproducibility Checklist
Movies S1 and S2

Submitted 27 February 2023; accepted 30 June 2023
Published online 13 July 2023
10.1126/science.adh3694